

# Rice grain disease identification using dual phase convolutional neural network-based system aimed at small dataset

Tashin Ahmed, Chowdhury Rafeed Rahman, Md. Faysal Mahmud Abid, and

United International University, Dhaka, Bangladesh

tahmed153109@bscse.uuu.ac.bd, rafeed@cse.uuu.ac.bd, fmaabid@gmail.com

**Abstract.** Although Convolutional neural networks (CNNs) are widely used for plant disease detection, they require a large number of training samples when dealing with wide variety of heterogeneous background. In this work, a CNN based dual phase method has been proposed which can work effectively on small rice grain disease dataset with heterogeneity. At the first phase, Faster RCNN method is applied for cropping out the significant portion (rice grain) from the image. This initial phase results in a secondary dataset of rice grains devoid of heterogeneous background. Disease classification is performed on such derived and simplified samples using CNN architecture. Comparison of the dual phase approach with straight forward application of CNN on the small grain dataset shows the effectiveness of the proposed method which provides a 5 fold cross validation accuracy of 88.07%.

**Keywords:** Faster RCNN · Dual phase detection · Small dataset · Rice grain · Convolution

## 1 Introduction

As rice grain diseases occur at the very last moment ahead of harvesting, it does major damage to the cultivation process. The average loss of rice due to grain discolouration was 18.9% in India [4]. Yield losses caused by False Smut (FS) ranged from 1.01% to 10.91% in Egypt [1]. 75% yield loss of grain occurred in India in 1950, while in the Philippines more than 50% yield loss was recorded [21]. [15] showed detailed damage for different kinds of rice grain in Bangladesh for the year 2014. Rice yield loss is a direct consequence of Neck Blast (NB) disease, since this disease results in poor panicles. A big reason behind Neck Blast is an extreme phase of the Blast and grain disease [15]. [20] presented a detailed outcome from False Smut in Bangladesh from the year 2000 - 2017 which demonstrated how destructive the False Smut disease can be.

Collecting field level data on agronomy is a challenging task in the context of poor and developing countries. The challenges include lack of equipment and specialists. Farmers of such areas are ignorant of technology use which makes it quite difficult to collect crop disease related data efficiently using smart devices

via the farmers. Hence, scarcity of plant disease oriented data is a common challenge while automating disease detection in such areas.

Many researches have been undertaken with a view to automating plant disease detection utilizing different techniques of machine learning and image processing. [23] proposed a system with the ability to identify areas which contain abnormalities. They applied a threshold-based clustering algorithm for this task. [26] created a framework for the detection of defected diseased leaf using K-Means clustering based segmentation. They claimed that their approach was able to detect the healthy leaf area and defected diseased area accurately. [9] worked on *Bakanae gibberella fujikuroi* disease. They developed a genetic algorithm which was used for selecting essential traits and optimal model parameters for the SVM classifiers. A technique to classify the diseases based on percentage of RGB value of the affected portion was proposed by [14] utilizing image processing. A similar technique using multi-level colour image thresholding was proposed by [5] for RLB disease detection. Deep learning based object classification and segmentation has become the state-of-the-art for automatic plant disease detection. Neural network was employed by [3] for leaf disease recognition while a self organizing map neural network (SOM-NN) was used to classify rice disease images by [22]. [2] experimented with AlexNet CNN architecture to distinguish among 3 classes of rice disease using a small dataset containing 227 images. A similar research for classifying 10 classes of rice disease on a 500 image dataset was undertaken by [18] using a handmade deep CNN architecture. [7] demonstrated the benefit of using pre-trained model of AlexNet and GoogleNet when the training data is not large. Their dataset consisted of 9 diseases of tomatoes. [24] demonstrated a detailed comparative analysis of different state-of-the-art CNN baseline and finely tuned architecture on eight classes of rice disease and pest. They demonstrated two stage training approach for memory efficient small CNN architectures. Besides these works on rice disease, [12] developed specialized deep learning models based on specific CNN architectures for identification of plant leaf diseases with a dataset containing 58 classes from 25 different plants. On the other hand, [6] applied transfer learning on GoogleNet on a dataset containing 87848 images of 56 diseases infecting 12 plants. [27] claimed that extraction of disease region from the leaf image was the driving step, for which they have studied and compared various segmentation techniques. Some of the image segmentation algorithms were compared by [11] in order to segment the diseased portion of rice leaves.

Though the above mentioned researches have significant contribution in disease detection automation, none of the works addressed the problem of scarcity of data which limits the performance of CNN based architectures. Most of the researches focused on image augmentation techniques to tackle the dataset size issue. But applying different geometric augmentations on small size images result in nearly the same type of image production which has drawbacks in terms of neural network training [17, 28]. [10] showed how the production of similar images through augmentation can cause overfitting.

This research uses 200 images for three separate classes - Neck Blast, False Smut and Healthy grain mentioned in **Table 1**. The first phase of our proposed method deals with a learning oriented segmentation based architecture. This architecture helps in detecting the significant grain portion of a given image which has heterogeneous background. which is an easier task compared to disease localization. The detected grain portions cropped from the original image are used as separate simplified images. In the second phase, these simplistic grain images are used in order to detect grain disease using fine tuned CNN architecture. Because of the simplicity of the tasks assigned in the two phases, our proposed method performs well in spite of having only 200 images of three classes.

## 2 Our Dataset

Our balanced dataset of 200 images consists of three classes - False Smut, Neck Blast and healthy grain class as shown in Table 1. A sample image from each class has been shown in Figure 1. **Neck Blast** is generally caused by the fungus known as *Magnaporthe oryzae*. It causes plants to develop very few or no grains at all. Infected nodes result in panicle break down [31]. **False Smut** is caused by the fungus called *Ustilaginoidea virens*.<sup>1</sup> It results in lower grain weight and reduction of seed germination [16].

Data have been collected from two separate sources for this experiment - field data supervised by officials from Bangladesh Rice Research Institute (BRRI) and image data from the repository of [24]. As Boro species have the maximum threat to be affected with False Smut and Neck Blast, Boro rice plant has been chosen for experimental data collection [19]. Parameters like light, distance and uniqueness have been taken into consideration while capturing the photographs. Supplementary public data related to the paper can be found at [https://drive.google.com/drive/folders/1AJZdWu-\\_VTXNvJZTNAF0kciI5g8N97mJ?usp=sharing](https://drive.google.com/drive/folders/1AJZdWu-_VTXNvJZTNAF0kciI5g8N97mJ?usp=sharing)

Class	Image Count	Image Percentage
False Smut	75	37.50%
Neck Blast	63	31.50%
Healthy	62	31.00%

Table 1: Our Primary Dataset

<sup>1</sup> Rice Knowledge Bank



Fig. 1: Mentioned Three Classes

### 3 Materials and Methods

#### 3.1 Experimental Setup

**Hardware** For the training environment, assistance has been taken from two different sources.

- Royal Melbourne Institute of Technology (**RMIT**) provides GPU for international research enthusiasts and they provided a Red Hat Enterprise Linux Server along with the processor Intel Xeon E5-2690 CPU, clock speed of 2.60 GHz. It has 56 CPUs with two threads per core, 503 GB of RAM. Each user can use up to 1 petabyte of storage. There are also two 16 GB NVIDIA Tesla P100-PCIE GPUs available. First phase was completed through this server.
- Google Colab (Tesla K80 GPU, 12GB RAM) and Kaggle kernel (Tesla P100 GPU) have been used for counter experimentation.

**Our Models** Experiments have been performed using five state-of-the-art CNN architectures described as follows.

**VGG 16** is a sequential architecture consisting of 16 convolutional layers. Kernel size in all convolution layers is three [29].

**VGG19** has three extra convolutional layers and the rest is the same as VGG16 [29].

**ResNet50** belongs to the family of residual neural networks. It is a deep CNN architecture with skip connections and batch normalization [13]. The skip connections help in eliminating the gradient vanishing problem.

**InceptionV3** is a CNN architecture with parallel convolution branching [30]. Some of the branches have filter size as large as  $7 \times 7$ .

**Xception** takes the principles of Inception to an extreme. Instead of partitioning the input data into several chunks, it maps the spatial correlations for each output channel separately and performs  $1 \times 1$  depthwise convolution [8].

Hyperparameter	Tuned Value
Anchor Box Count	9 <b>16</b>
Anchor Box Size (pixel)	<b>32, 64, 128, 256</b> 128, 256, 512
Anchor Box Ratios	(1,1), (2,1), (1,2) <b>(1,1), (<math>\frac{1}{\sqrt{2}}, \frac{2}{\sqrt{2}}</math>), (<math>\frac{2}{\sqrt{2}}, \frac{1}{\sqrt{2}}</math>), (2,2)</b>
RPN Threshold	0.3 - 0.7 <b>0.4 - 0.8</b>
Proposal Selection	<b>200</b> 2000
Overlap Threshold	> <b>0.8</b> >0.9
Learning Rate	0.001 <b>0.0001</b> 0.00001
Optimizers	<b>Adam</b> SGD

Table 2: List of hyperparameters tuned using 5 fold cross validation. Bold values represent selected values for the final results

**Tuned Hyperparameters** Hyperparameters of the CNN based architecture shown in Table 2 are described as follows.

**Anchor Box Hyperparameters:** Anchor boxes are a set of bounding boxes defined through different scales and aspect ratios. They mark the probable regions of interest of different shapes and sizes. The total number of probable anchor boxes per pixel of a convolutional feature map is  $P_n \times R_n$ , where  $P_n$  and  $R_n$  denote the number of anchor box size variations and ratio variations respectively.

**Region Proposal Network (RPN) Hyperparameters:** RPN layer utilizes the convolutional feature map of the original image to propose regions of interest that are identifiable within the original image. The proposals are made in line with the anchor boxes. For each anchor box, RPN predicts if it is an object of interest or not and changes the size of the anchor box to better fit the object. RPN threshold of 0.4 - 0.8 means that any proposed region which has IoU (Intersection Over Union) less than 0.4 with ground truth object is considered a wrong guess whereas any proposed region which has IoU greater than 0.8 with ground truth object is considered correct. This notion is used for training the RPN layer.

**Proposal Selection:** Proposal selection threshold of 200 means that top (according to probability) 200 region proposals from RPN layer will pass on to the next layers for further processing.

**Overlap Threshold:** During non-max suppression, overlapping object proposals are excluded if the IoU is above a certain threshold. If their overlap is greater than the threshold, only the proposal with the highest probability is

kept and the procedure continues until there are no more boxes with sufficient overlap.

**Learning Rate:** It is used for controlling the speed of model parameter update.

**Optimizer:** Optimizer is an algorithm for updating model parameter weights after training on each batch of samples. Weight updating process varies with the choice of optimizer.

### 3.2 Proposed Dual Phase Approach

In this research, dual phase approach has been introduced in order to learn effectively from small dataset containing images with a lot of heterogeneity in the background. The approach overview has been provided in Figure 2. In the first phase, the original image is taken, reshaped to a fixed size and then passed through segmentation oriented Faster RCNN architecture. Localizing and classifying the diseases using Faster RCNN alone would be next to impossible because of the lack of large dataset [25]. Since this architecture has been trained only to localize the significant grain portion (a fairly simple task), it performs well even with such small dataset. After obtaining the significant grain portions from an image, those regions are cropped and resized to a fixed size. These images look simple because of the absence of heterogeneous background. CNN architecture is trained on this simplified dataset to detect disease. The learning process has been shown to be effective through experiments.

### 3.3 Segmenting Grain Portion

This is the first phase of our approach. Segmentation algorithms based on CNN architecture as a backbone requires image to be of fixed size. Input images have been resized to  $640 \times 480$  before feeding them to Faster RCNN. The consecutive stages of the network through which this resized image passes through have been described as follows.

#### Convolutional neural network (CNN)

In order to avoid sliding a window in each spatial position of the original image, CNN architecture is used in order to learn and extract feature map from the image which represents the image effectively. The spatial dimension of such feature map decreases whereas the channel number increases. For the dataset used in this research, VGG16 architecture has proven to be the most effective. Hence, VGG16 has been used as the backbone CNN architecture which transforms the original image into  $20 \times 15 \times 512$  dimension.

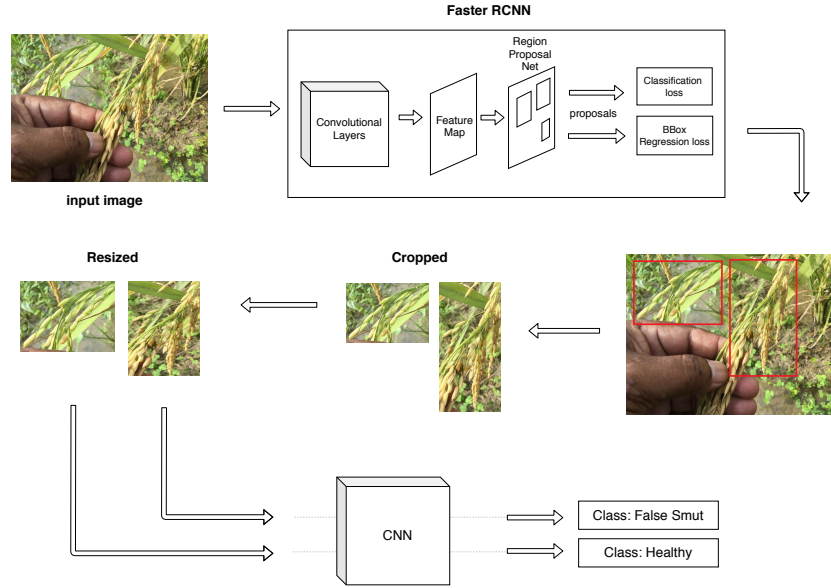


Fig. 2: Dual Phase Approach

### Region Proposal Network (RPN)

The extracted feature map is passed through RPN layer. For each pixel of the feature map of spatial size  $20 \times 15$ , there are 16 possible bounding boxes (4 different aspect ratios and 4 different sizes mentioned in bold letter in Table 2). So, that makes total  $16 \times 20 \times 15 = 4800$  possible bounding boxes, RPN is a two branch Convolution layer which provides two scores (branch one) and four coordinate adjustments (branch two) for each of the 4800 boxes. The two scores correspond to the probability of being an object and a non-object. Only those boxes which have a high object probability are taken into account. Non-max suppression (NMS) is used in order to eliminate overlapping object bounding boxes and to keep only the high probability unique boxes. The threshold of this overlap in this case is 0.8 IoU. From this probable object proposals, top 200 proposals according to object probability are passed to the next layers.

### ROI Pooling

Each of the 200 selected object proposals correspond to some region in the CNN feature map. For passing each of these regions on to the dense layers of the architecture, each of the regions need to be of fixed size. ROI pooling layer takes each region and turns them into  $7 \times 7 \times 512$  using bilinear interpolation and max pooling.

### RCNN Layer

RCNN layer consists of fully connected dense layers. Each of the  $7 \times 7 \times 512$  size feature maps are flattened and passed through these fully connected

layers. The final layer has two branches. Branch one predicts if the input feature map is background class or significant grain portion. Branch two provides four regression values denoting the adjustment of the bounding box to better fit the grain portion. For each feature map, if the probability of being a grain is over 0.6, only then is the feature map considered as a probable grain portion and the adjusted coordinates are mapped to the original image in order to get the localized grain portion. The overlapping boxes are eliminated using NMS. The remaining bounding box regions are the significant grain portions.

### Loss Function

The trainable layers of Faster RCNN architecture are: CNN backbone, RPN layer and RCNN layer. A loss function is needed in order to train these layers in an end to manner which is as follows.

$$L(p_i, t_i) = \frac{1}{N_{cls}} \sum_i L_{cls}(p_i, p_i^*) + \lambda \frac{1}{N_{reg}} \sum_i p_i^* L_{reg}(t_i, t_i^*)$$

The first term of this loss function defines the classification loss over two classes which describe whether predicted bounding box  $i$  is an object or not. The second term defines the regression loss of the bounding box when there is a ground truth object having significant overlap with the box. Here,  $p_i$  and  $t_i$  denote predicted object probability of bounding box  $i$  and predicted four coordinates of that box respectively while  $p_i^*$  and  $t_i^*$  denote the same for the ground truth bounding box which has enough overlap with predicted bounding box  $i$ .  $N_{cls}$  is the batch size (256 in this case) and  $N_{reg}$  is the total number of bounding boxes having enough overlap with ground truth object. Both these terms work as normalization factor.  $L_{cls}$  and  $L_{reg}$  are log loss (for classification) and regularized loss (for regression) function respectively.

### 3.4 Disease Detection from Segmented Grain

Figure 2 shows Faster RCNN architecture drawing bounding boxes on two significant grain portions. These portions are cropped and resized to a fixed size ( $200 \times 250$  in this case) in order to pass each of them through a CNN architecture. Thus two images have been created from single image of the primary original dataset. The same process can be executed on each of the images of the primary dataset. Thus a secondary dataset of significant grain portion can be created. Each of these images have to be labeled as one of the three classes in order to train the CNN architecture. The complete dataset including these secondary image counts has been shown in Table 3. The cropped portions when passed through a trained CNN model have been predicted as False Smut disease and healthy grain class in Figure 2. As a result, the final decision is that the original image of this figure is infected by False Smut disease.



Classes	Image Count (Primary)	Image Count (Secondary)	Image Increment
False Smut	75	85	10
Neck Blast	63	70	7
Healthy	62	64	3
Total	200	219	19

Table 3: Complete Dataset

## 4 Results and Discussion

All results have been provided in terms of 5 fold cross validation. **Accuracy** has been used in order to compare dual phase approach against implementation of CNN on original images without any segmentation. Accuracy is a good measure for balanced dataset.

$$Accuracy = \frac{TP}{TP + FP + TN + FN}^2$$

Segmenting the grain portion is the goal of the first phase of the dual phase approach. For evaluating the performance of this phase, **mAP** (mean average precision) score has been used. Precision, recall and IoU (Intersection over Union) are required to calculate mAP score.

$$Precision = \frac{TP}{TP + FP}$$

$$Recall = \frac{TP}{TP + FN}$$

$$IoU = \frac{AOI}^3 AOU$$

If a predicted box IoU is greater than a certain threshold, it is considered as TP. Otherwise, it is considered as FP.  $(TP + FN)$  is actually the total number of ground truth bounding boxes. Average precision (AP) is calculated from the area under the precision-recall curve. If there are N classes, then mAP is the average AP of all these classes. In this research, there is only one class of object in phase one, that is the significant grain portion class. So, here AP and mAP are the same.

[24] showed the effectiveness of fine tuned CNN architectures for rice dataset. As a result, fine tuning was used in this research to achieve the best possible outcome. Results obtained from the straightforward use of fine tuned CNN architectures on the small grain dataset have been shown in Table 4. Here, VGG16

<sup>2</sup> TP: True Positive, FP: False Positive, TN: True Negative, FN: False Negative

<sup>3</sup> AOI: Area of intersection, AOU: Area of union (with respect to ground truth bounding box)

stands out with the accuracy of 75.60%, which is not satisfactory. Rest of the architectures have gained accuracy of less than 70%. Since VGG16 has shown the best performance on this dataset, the rest of the experiments have been performed using VGG16.

CNN Architecture	Validation Accuracy	Standard Deviation
VGG16	75.6%	4.39
ResNet50	66.6%	3.36
InceptionV3	59.6%	5.68
Xception	58.4%	6.02
VGG19	68.6%	4.03

Table 4: Straightforward CNN Implementation Results

The mAP scores for different hyperparameter values have been provided in Table 5. The best mAP score achieved is 88.24% with configuration two (any mAP score above 80% is impressive). The significant grain portions have been cropped using this configuration. Phase two experiment using CNN architecture has been performed on this cropped portions. Table 4 shows that VGG16 and ResNet50 have performed best among sequential and non-sequential CNN architectures respectively. As a result, phase two training and validation have been performed with these two architectures. Results have been shown in Figure 6. VGG16 has achieved an impressive accuracy of 88.07% with small grain dataset.

CNN Architecture	Anchor Box Ratios	Anchor Box Pixels	RPN Threshold	Overlap Threshold	Val mAP	Std. dev
VGG16	(1:1), (2:1), (1:2)	128, 256, 512	0.3 - 0.7	>0.8	79.95%	1.00
VGG16	(1:1), ( $\frac{1}{\sqrt{2}} : \frac{2}{\sqrt{2}}$ ), ( $\frac{2}{\sqrt{2}} : \frac{1}{\sqrt{2}}$ ), (2:2)	32, 64, 128, 256	0.4 - 0.8	>0.8	88.24%	2.16
VGG16	(1:1), ( $\frac{1}{\sqrt{2}} : \frac{2}{\sqrt{2}}$ ), ( $\frac{2}{\sqrt{2}} : \frac{1}{\sqrt{2}}$ ), (2:2)	32, 64, 128, 256	0.4 - 0.8	>0.9	87.08%	2.49

Table 5: Phase One Results

The result from the second phase was generated using VGG16 and ResNet50 where VGG16 stands out with the accuracy of 88.07%  $\pm$ 1.96%.

CNN Architecture	Validation Accuracy	Standard Deviation
VGG16	88.07%	1.96
ResNet50	81.39%	1.98

Table 6: Phase Two Results

As can be seen from Figure 3, the images of the primary dataset have large portion of heterogeneous background. This characteristic will remain true in all plant disease images collected in real life scenario. Such heterogeneity makes it difficult for straightforward use of CNN architecture to achieve good results. In case of the dual phase approach proposed, this difficult task has been divided into two simple tasks. First task is to localize the significant grain portion shown in red boxes in Figure 3. The second task involves disease classification from these red marked bounding box regions which do not contain any significant background portion. As a result, proposed approach has been able to perform well on a small dataset collected in real life scenario.

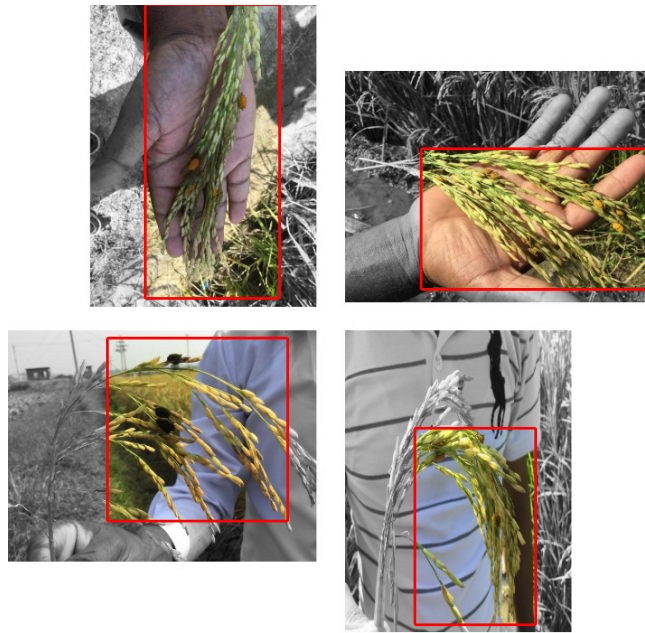


Fig. 3: Primary Dataset Image Background (Shaded)

## 5 Conclusion

In brief, this research has the following contributions:

- A dual phase approach capable of learning from small rice grain disease dataset has been proposed.
- A smart segmentation procedure has been proposed in phase one which is capable of handling heterogeneous background prevalent in plant disease image dataset collected in real life scenario.

- Experimental comparison has been provided with straightforward use of state-of-the-art CNN architectures on the small rice grain dataset to show the effectiveness of the proposed approach.

## 6 Acknowledgments

We thank Bangladesh Information and Communications Technology (ICT) division for aiding this research. We also thank the authority of Bangladesh Rice Research Institute (BRRI) for supporting us with field level data collection. We also acknowledge the help of RMIT University who gave us the opportunity to use their GPU server. We would like to thank Laila Sultana (laila.sultana.esms@gmail.com), Ummea Sarah Ali (uali151098@bscse.uui.ac.bd) and Abdullah Al Noman (anoman143062@bscse.uui.ac.bd) for helping us with data collection and labeling.

## References

1. Atia, M.: Rice false smut (*ustilagoidea virens*) in egypt. *Journal of Plant Diseases and Protection* **111**(1), 71–82 (2004)
2. Atole, R.R., Park, D.: A multiclass deep convolutional neural network classifier for detection of common rice plant anomalies. *INTERNATIONAL JOURNAL OF ADVANCED COMPUTER SCIENCE AND APPLICATIONS* **9**(1), 67–70 (2018)
3. Babu, M.P., Rao, B.S., et al.: Leaves recognition using back propagation neural network-advice for pest and disease control on crops. *IndiaKisan. Net: Expert Advisory System* (2007)
4. Baite, M.S., Raghu, S., Prabhukarthikeyan, S., Keerthana, U., Jambhulkar, N.N., Rath, P.C.: Disease incidence and yield loss in rice due to grain discolouration. *Journal of Plant Diseases and Protection* pp. 1–5 (2019)
5. Bakar, M.A., Abdullah, A., Rahim, N.A., Yazid, H., Misman, S., Masnan, M.: Rice leaf blast disease detection using multi-level colour image thresholding. *Journal of Telecommunication, Electronic and Computer Engineering (JTEC)* **10**(1-15), 1–6 (2018)
6. Barbedo, J.G.A.: Impact of dataset size and variety on the effectiveness of deep learning and transfer learning for plant disease classification. *Computers and electronics in agriculture* **153**, 46–53 (2018)
7. Brahimi, M., Boukhalfa, K., Moussaoui, A.: Deep learning for tomato diseases: classification and symptoms visualization. *Applied Artificial Intelligence* **31**(4), 299–315 (2017)
8. Chollet, F.: Xception: Deep learning with depthwise separable convolutions. In: *Proceedings of the IEEE conference on computer vision and pattern recognition*. pp. 1251–1258 (2017)
9. Chung, C.L., Huang, K.J., Chen, S.Y., Lai, M.H., Chen, Y.C., Kuo, Y.F.: Detecting bakanae disease in rice seedlings by machine vision. *Computers and electronics in agriculture* **121**, 404–411 (2016)
10. Cogswell, M., Ahmed, F., Girshick, R., Zitnick, L., Batra, D.: Reducing overfitting in deep networks by decorrelating representations. *arXiv preprint arXiv:1511.06068* (2015)

11. Devi, D.A., Muthukannan, K.: Analysis of segmentation scheme for diseased rice leaves. In: 2014 IEEE International Conference on Advanced Communications, Control and Computing Technologies. pp. 1374–1378. IEEE (2014)
12. Ferentinos, K.P.: Deep learning models for plant disease detection and diagnosis. *Computers and Electronics in Agriculture* **145**, 311–318 (2018)
13. He, K., Zhang, X., Ren, S., Sun, J.: Deep residual learning for image recognition. In: Proceedings of the IEEE conference on computer vision and pattern recognition. pp. 770–778 (2016)
14. Islam, T., Sah, M., Baral, S., RoyChoudhury, R.: A faster technique on rice disease detection using image processing of affected area in agro-field. In: 2018 Second International Conference on Inventive Communication and Computational Technologies (ICICCT). pp. 62–66. IEEE (2018)
15. Khan, M.A.I., Bhuiyan, M.R., Hossain, M.S., Sen, P.P., Ara, A., Siddique, M.A., Ali, M.A.: Neck blast disease influences grain yield and quality traits of aromatic rice. *Comptes rendus biologiques* **337**(11), 635–641 (2014)
16. Koiso, Y., Li, Y., Iwasaki, S., HANAKA, K., Kobayashi, T., Sonoda, R., Fujita, Y., Yaegashi, H., Sato, Z.: Ustiloxins, antimitotic cyclic peptides from false smut balls on rice panicles caused by *Ustilagoidea virens*. *The Journal of antibiotics* **47**(7), 765–773 (1994)
17. Liu, R., Gillies, D.F.: Overfitting in linear feature extraction for classification of high-dimensional image data. *Pattern Recognition* **53**, 73–86 (2016)
18. Lu, Y., Yi, S., Zeng, N., Liu, Y., Zhang, Y.: Identification of rice diseases using deep convolutional neural networks. *Neurocomputing* **267**, 378–384 (2017)
19. Miah, S., Shahjahan, A., Hossain, M., Sharma, N.: A survey of rice diseases in bangladesh. *International Journal of Pest Management* **31**(3), 208–213 (1985)
20. Nessa, B.: Rice False Smut Disease in Bangladesh: Epidemiology, Yield Loss and Management. Ph.D. thesis, PhD thesis, Department of Plant Pathology and Seed Science, Sylhet (2017)
21. Ou, S.H.: Rice diseases. IRRI (1985)
22. Phadikar, S., Sil, J.: Rice disease identification using pattern recognition techniques. In: 2008 11th International Conference on Computer and Information Technology. pp. 420–423. IEEE (2008)
23. Pugoy, R.A.D., Mariano, V.Y.: Automated rice leaf disease detection using color image analysis. In: Third International Conference on Digital Image Processing (ICDIP 2011). vol. 8009, p. 80090F. International Society for Optics and Photonics (2011)
24. Rahman, C.R., Arko, P.S., Ali, M.E., Khan, M.A.I., Apon, S.H., Nowrin, F., Wasif, A.: Identification and recognition of rice diseases and pests using convolutional neural networks. arXiv preprint arXiv:1812.01043 (2018)
25. Ren, S., He, K., Girshick, R., Sun, J.: Faster r-cnn: Towards real-time object detection with region proposal networks. In: Advances in neural information processing systems. pp. 91–99 (2015)
26. Sethy, P.K., Negi, B., Bhoi, N.: Detection of healthy and defected diseased leaf of rice crop using k-means clustering technique. *International Journal of Computer Applications* **157**(1), 24–27 (2017)
27. Shah, J.P., Prajapati, H.B., Dabhi, V.K.: A survey on detection and classification of rice plant diseases. In: 2016 IEEE International Conference on Current Trends in Advanced Computing (ICCTAC). pp. 1–8. IEEE (2016)
28. Shorten, C., Khoshgoftaar, T.M.: A survey on image data augmentation for deep learning. *Journal of Big Data* **6**(1), 60 (2019)

29. Simonyan, K., Zisserman, A.: Very deep convolutional networks for large-scale image recognition. arXiv preprint arXiv:1409.1556 (2014)
30. Szegedy, C., Vanhoucke, V., Ioffe, S., Shlens, J., Wojna, Z.: Rethinking the inception architecture for computer vision. In: Proceedings of the IEEE conference on computer vision and pattern recognition. pp. 2818–2826 (2016)
31. Wilson, R.A., Talbot, N.J.: Under pressure: investigating the biology of plant infection by *magnaporthe oryzae*. *Nature Reviews Microbiology* **7**(3), 185–195 (2009)